
FOR THE RECORD

Contribution of the intrinsic disulfide to the assembly mechanism of islet amyloid

BON W. KOO AND ANDREW D. MIRANKER

Department of Molecular Biophysics and Biochemistry, Yale University, New Haven, Connecticut 06520-8114, USA

(RECEIVED August 10, 2004; FINAL REVISION August 10, 2004; ACCEPTED September 13, 2004)

Abstract

Amyloidogenesis from soluble protein requires conformational and oligomeric assembly steps. In systems where the precursor protein is natively unfolded, such as islet amyloid polypeptide (IAPP), forces and structural changes relevant to protein unfolding are not thought to participate in the assembly mechanism. Thus, fiber core structure elements should provide the dominant contributions to assembly kinetics. Here we show, however, that residues outside the amyloid core can influence the mechanism of IAPP fiber assembly. IAPP possesses an intramolecular disulfide bond between residues 2 and 7. This short-range disulfide prohibits the N-terminal region from adopting the β -strand structure of an amyloid. We examined the role of this disulfide in fiber formation by generating a truncated construct (IAPP₈₋₃₇) and a stable reduced form of the full-length protein (IAPP_{CAM}). The fiber structures and assembly kinetics of these variants were assessed via optical and mass spectroscopy. Our data confirm that the disulfide does not contribute to the amyloid fiber core structure. Remarkably, however, it plays a central role in the assembly mechanism. First, loss of the disulfide substantially reduces fiber formation by secondary nucleation, i.e., the ability of pre-existing fibers to participate in the formation of new fibers. Second, the bypass of nucleation by seed addition is a two-step process, termed activation. Loss of the disulfide eliminates this two-step nature of seeded kinetics.

Keywords: amylin; amyloid; islet amyloid polypeptide; protein folding; secondary nucleation, phase-mediated fibrillogenesis; type II diabetes

The oligomerization of soluble protein into large, highly ordered fibrillar structures, termed amyloids, is a common feature of a number of diseases including, for example, Alzheimer's disease and dialysis-related amyloidosis (Rochet and Lansbury 2000). Interestingly, proteins that undergo amyloid fiber formation vary greatly in their native structures and functions, but in the fiber state, exhibit common features. Amyloid fibers form a core that is predominantly composed of β -sheets. The strands within these sheets are organized perpendicular to the long axis of the

fiber with backbone hydrogen bonding oriented in parallel to the fiber axis (Eanes and Glenner 1968; Sunde and Blake 1997). The common core structure of amyloids suggests that assembly mechanisms across different systems are comparable. Indeed, the overall kinetic behaviors of amyloids also share common features. A protein placed under amyloidogenic conditions will initially remain soluble. This quiescent phase, termed the lag phase, is followed by collective assembly into the aggregated state. This implies the existence of nucleation processes akin to crystallization (Harper and Lansbury 1997). As with crystallization, nucleation reactions within the lag phase may be bypassed by providing exogenous fiber from a previously conducted reaction. A number of intermediate states likely participate in the assembly process. As amyloidogenesis occurs in a variety of biomedical systems with unrelated primary se-

Reprint requests to: Andrew Miranker, Department of Molecular Biophysics and Biochemistry, Yale University, 260 Whitney Ave., New Haven, CT 06520-8114, USA; e-mail: Andrew.Miranker@yale.edu; fax: (203) 432-5175.

Article published online ahead of print. Article and publication date are at <http://www.proteinscience.org/cgi/doi/10.1110/ps.041051205>.

quence, it is vital to elucidate these states in order to determine a generalized basis for assembly. In addition, recent studies suggest that it is the intermediates of fiber formation which are the cytotoxic species (Bucciantini et al. 2002). Thus, insights into amyloid assembly mechanisms are essential to developing our understanding of the intrinsic physical properties of polypeptides, and to developing effective targets for therapeutics.

Islet amyloid polypeptide (IAPP), or amylin, is a peptide hormone that is normally co-secreted with insulin by the β cells of the pancreas. In patients with type II diabetes, unmodified IAPP deposits as cytotoxic amyloid in the extracellular spaces of the pancreatic islets (Kahn et al. 1999). In its soluble form, IAPP is an unstructured (Kayed et al. 1999; Higham et al. 2000), C-terminally amidated 37-residue peptide containing an intramolecular disulfide bond between residues 2 and 7. Generally, the energies governing amyloid formation include those associated with unfolding of the precursor and those of stabilizing the fiber. For many amyloid systems, including IAPP, the precursor is intrinsically unstructured. For such proteins, the forces that define the assembly pathway are derived from the fiber structure itself. In IAPP, for example, fluorescence resonant energy transfer (FRET) has been used to identify long-range aromatic interactions in the mature fiber. Interestingly, these interactions are also transiently sampled by prefibrillar conformations of IAPP (Padrick and Miranker 2001). Previous work on IAPP has also identified a number of events in the process of fiber assembly. In this work, we address two of these. First, we previously reported that the process of IAPP fiber formation follows a double-nucleation mechanism (DNM) of fibrillogenesis (Padrick and Miranker 2002); i.e., there are mechanisms for both fiber-independent (primary nucleation) and fiber-dependent (secondary nucleation) means for increasing the molar concentration of fiber ends. Second, we demonstrated the presence of an activation step evident during the lag phase of fiber formation (Padrick and Miranker 2002). This is visible in the kinetic profile of seeded fiber formation. Briefly, addition of seed at the beginning of a fibrillogenesis reaction gives rise to a sigmoidal reaction profile. If instead seed is added several minutes after initiation of the reaction, single-phase exponential profiles are observed. Similar two-phase kinetics for seeded polymerization have been observed *in vitro* for yeast prion protein Sup35p (Santoso et al. 2000).

It is challenging to reconcile the presence of a minute timescale kinetic event with the dynamics of an unstructured polypeptide. Human IAPP does not possess any proline residues. The longest timescale available for conformational change should therefore be of the order of μ sec (Plaxco and Dobson 1996; Kubelka et al. 2004) and not minutes. As the overall unfolded structure of prefibrillar IAPP has been determined by far-UV CD (Kayed et al. 1999; Higham et al. 2000), it is plausible that local struc-

tures play an important role, for example, aromatic interactions (Padrick and Miranker 2001; Gazit 2002). In this work, we examined the role of the N-terminal disulfide. In human IAPP, this disulfide bond spans residues 2–7. A five-residue span renders this region of the polypeptide incapable of forming canonical secondary structures. Nevertheless, we can report that perturbations occur to the assembly kinetics of IAPP fibers upon removal of this disulfide. These alterations shed light on the mechanism of IAPP fibrillogenesis.

Results

IAPP readily forms fibers upon dilution of the protein from a concentrated (1–3 mM) stock solution in HFIP into physiological buffer (pH 7.4, 100 mM KCl, 50 mM potassium phosphate). Kinetics are monitored using the change in the anisotropy of the intrinsic tyrosine at residue 37. A hallmark of fiber formation kinetics is the capacity to bypass nucleation by the addition of exogenous seed. For IAPP, addition of as little as 1 μ M seed (in monomer units) to a 10 μ M reaction results in fiber formation reaching completion on the timescale of the lag phase of its *de novo* counterpart (Fig. 1). The wholesale bypass of the lag phase indicates that primary nucleation phenomena contribute little to the seeded kinetic profile. Nevertheless, the profile of seeded kinetics retains a sigmoidal shape indicative of processes additional to elongation. The timescale of this additional process can be estimated by conducting a seeded reaction in which seed is added several minutes after initiation of the *de novo* reaction. Addition of seed 45 min after initiation of the *de novo* reaction results in an exponential kinetic profile (Fig. 1). Thus, we can infer that soluble IAPP undergoes conformational transitions on the minute-timescale. To test the possibility that the N-terminal region of the peptide is important for this slow activation event observed in seeded kinetics, we generated an N-terminal truncation consisting of residues 8 to 37 of IAPP (IAPP_{8–37}) (Fig. 2). This variant eliminates the disulfide, but also eliminates several other residues including a charged residue, Lys 1. Therefore, we also generated a reduced and blocked variant of full-length IAPP by reacting the free thiols at residues 2 and 7 with iodoacetamide, resulting in the formation of a carboxyamidomethyl (CAM) blocked protein (IAPP_{CAM}) (Fig. 2). Structure at the molecular level was inferred using optical and mass spectroscopies, and fiber formation was assessed by performing measurements of *de novo*, seeded, and cross-seeded assembly kinetics.

IAPP_{8–37} and IAPP_{CAM} readily form amyloid fibrils *in vitro*. Wild-type IAPP (IAPP_{WT}), IAPP_{8–37}, and IAPP_{CAM} were incubated for 1 h under our standard reaction conditions (see Materials and Methods). These conditions are known to generate fibers from wild-type protein (Padrick and Miranker 2001, 2002) and are similar to conditions

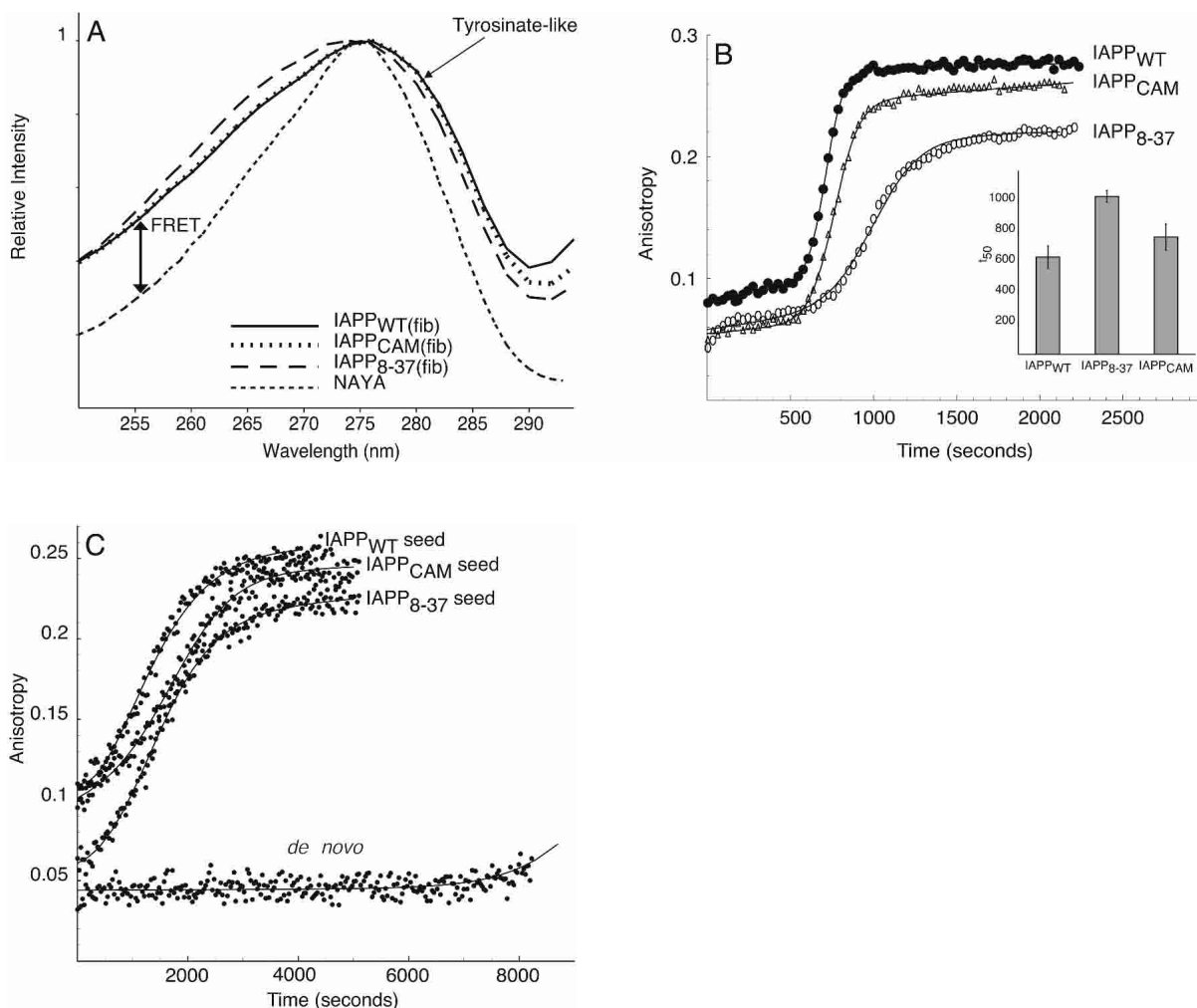


Figure 3. (A) Assessment of fiber formation and fiber structure by FRET. UV excitation spectra of the fiber states of the three protein constructs. Fiber samples were excited from 250 nm to 300 nm with emission detected at 303 nm. The excitation spectrum of N-acetyl-tyrosinamide is shown as a negative control. All three variants show the presence of characteristic enhancements: FRET from F15 and F23 are evident at 255 nm, whereas tyrosinate character is evident as a shoulder above 278 nm (Padrick and Miranker 2001). Fiber samples were generated under standard conditions (see Materials and Methods). (B) Kinetics of de novo fiber formation. Shown are the anisotropy data and fits for the three IAPP constructs. Each curve is representative of a triplicate set of data. Each reaction was performed under matched conditions (see Materials and Methods). (Inset) The midpoint of transition (t_{50}) for fiber formation reactions of each construct done in triplicate as obtained from fits of the anisotropy kinetics to sigmoidal curves (see Materials and Methods). (C) Kinetics of fiber formation of soluble IAPP_{WT} in the presence of IAPP_{WT}, IAPP₈₋₃₇, and IAPP_{CAM} fiber seeds. A total of four reactions are shown. For reference, a wild-type de novo reaction performed under matched conditions is shown. The kinetics of seeded IAPP fiber formation was assessed in the presence of preformed fibers of the three constructs: IAPP_{WT}, IAPP₈₋₃₇, and IAPP_{CAM}. Here, 1 μ M of each fiber seed sample (see Materials and Methods) was added to a reaction containing 10 μ M of soluble wild-type IAPP and 1.5% HFIP. Each kinetic curve was fit to a sigmoid transition, as described in Materials and Methods.

IAPP₈₋₃₇ and IAPP_{CAM} occurs on a timescale similar to that of the wild-type peptide under matched reaction conditions (Fig. 3B). Reported errors in timescale (Fig. 3B, inset) correspond to variation within a given stock solution of peptide. Stock-to-stock variability is typically within a factor of two. In addition, the protein concentration independence of wild-type IAPP fiber formation is not significantly perturbed for either IAPP_{CAM} or IAPP₈₋₃₇. For example, the t_{50} for IAPP₈₋₃₇ varies by less than a factor of two over a concentration range of 5 μ M to 15 μ M (data not shown). In

contrast, the t_{50} of a concentration-dependent polymerization reaction is expected to scale in inverse proportion to $[\text{precursor}]_0^{n/2}$ where n is the oligomeric size of the nucleus (Oosawa and Asakura 1975). That is, even assuming a minimal nucleus size of two molecules, a threefold change in t_{50} is expected.

Preformed fibrils of IAPP₈₋₃₇ and IAPP_{CAM} can effectively seed de novo fiber formation reactions of human wild-type IAPP. Seeding of fiber formation is a structurally specific process (Come et al. 1993; Chien and Weissman

2001; O’Nuallain et al. 2004). Extreme examples of this have been observed in both yeast and mammalian prions. For example, a single chimeric sequence of Sup35 formed from *C. albicans* and *S. cerevisiae* can generate alternative kinetic profiles depending on whether it is seeded by *C. albicans* or *S. cerevisiae* (Santoso et al. 2000). We performed cross-seeding experiments in which a small amount (1 μM) of seed material composed of one variant was used to seed fiber formation of 10 μM wild-type IAPP (Fig. 3C). Seeding of IAPP_{WT} by IAPP₈₋₃₇ and IAPP_{CAM} is comparable to self-seeding by IAPP_{WT} fiber in two ways. First, the timescales of cross-seeding are identical to the self-seeded reaction (Fig. 3C), when fiber samples are prepared under equivalent buffer conditions and concentrations. Second, the kinetic profiles of the cross-seeded reactions are two-phase and sigmoidal and mirror the profile for self-seeding. Similarly, we find that soluble IAPP₈₋₃₇ and IAPP_{CAM} can be cross-seeded by preformed IAPP_{WT} fibers (data not shown) on a timescale similar to self-seeding of IAPP₈₋₃₇ and IAPP_{CAM}. Therefore, the ability of IAPP₈₋₃₇ and IAPP_{CAM} to cross-seed fiber formation of soluble IAPP_{WT} further reflects structural similarities between the three constructs in the fiber state, specifically that the structural features of the fiber ends are equivalent to that of wild-type IAPP.

Removal of the disulfide bond eliminates the activation phase observed in seeded kinetics of wild-type IAPP. Seeded fiber formation reactions for each construct were conducted by adding 1 μM preformed fibers to a solution containing 10 μM soluble peptide of the same variant at the start of the reaction. De novo and seeded fiber formation reactions for each variant were performed using the same solution preparations and protein stocks in order to correlate the timescales of seeding reactions with their de novo counterparts. In order to facilitate this analysis, we renormalized the kinetics of seeded fiber formation to the t_{50} obtained from fits of the de novo reactions (Fig. 4). As described previously, we see that the kinetic profile of IAPP_{WT} seeded fiber formation is sigmoidal and reflects the presence of two fibril growth phases, an initial lag phase followed by a second faster phase (Fig. 4A). The sigmoidal nature of seeding can be illuminated by plotting the first derivative of the kinetic profile on a time-renormalized axis (t_{50} of unseeded reaction = 1, see inset, Fig. 4A). The sigmoidal shape of the kinetic profile results in a peak in the first derivative plot, as the rate of change of anisotropy (i.e., turnover rate for fiber formation) reaches a maximum at the t_{50} of the reaction. Interestingly, we observe significant changes to the kinetics of fiber formation in the absence of the disulfide bridge. Unlike IAPP_{WT} seeded kinetics, a seeded reaction containing a small amount (1 μM) of IAPP₈₋₃₇ fiber leads to a kinetic profile that follows an exponential decay (Fig. 4B). The seeded kinetics can be fit to an exponential decay model, and the change in kinetic profile is clearly portrayed

in the first derivative plot (Fig. 4B, inset). Similarly, the biphasic nature of seeding is also eliminated in the seeded kinetics of IAPP_{CAM} (Fig. 4C), and the first derivative plot (Fig. 4C, inset) clearly shows a change in kinetic behavior similar to IAPP₈₋₃₇ seeded fiber formation. The change in kinetic behavior observed for the two disulfide-free constructs therefore reflects a loss of the activation phase of fiber formation under our reaction conditions.

The removal of the disulfide bond leads to a significant loss in the sensitivity of the fibrillogenesis reaction to seeding. As shown in Figure 4A, kinetics of wild-type IAPP seeded fiber formation reach completion significantly before the t_{50} of its de novo counterpart. In contrast, seeding of IAPP₈₋₃₇ fiber formation takes place on a timescale that is comparable to the de novo counterpart (Fig. 4B). We observe a similar behavior for seeded IAPP_{CAM} fiber formation reactions (Fig. 4C). Plainly, the sensitivity of IAPP fiber formation to seed is greatly affected by removal of the disulfide bridge. Overall, such changes in seeded fiber formation kinetics indicate that the removal of the disulfide affects the mechanism by which IAPP fiber formation is accelerated by the presence of exogenous seed.

Disulfide modification gives rise to significant alterations in the relative contributions of different assembly processes. Wild-type IAPP polymerization kinetics deviate from primary nucleation-dependent polymerization (NDP) kinetics (Padrick and Miranker 2002). This is most evident on a time-renormalized plot (Fig. 5B) where the shape of NDP kinetics is insensitive to parameters such as reaction timescale (Fig. 5A). The relative steepness of IAPP’s polymerization transition reflects the presence of secondary nucleation. Note, that for IAPP, like NDP, the renormalized profile is consistent regardless of the actual timescale of the reaction. For example, the representative IAPP_{WT} reaction (Fig. 5A) performed in the presence of 1.5% HFIP has a t_{50} of 8000 sec, while at 2%, it has a t_{50} of 2500 sec. These reactions essentially overlay when time renormalized. For IAPP₈₋₃₇ and IAPP_{CAM} de novo reactions, however, we observe a significant change in the kinetic profiles (Fig. 5B). Plainly the profiles of these constructs are less abrupt and begin to approach a shape similar to that of NDP.

Discussion

Identifying the molecular nature of kinetic events in IAPP fiber formation is essential to understanding the mechanism of fiber assembly. In this work, we examined the impact of a nonamyloidogenic subdomain (residues 1–7) of IAPP on fibrillogenesis. Six observations affect our understanding of the wild-type protein. Comparisons of IAPP_{WT} with N-terminally modified constructs reveal: (1) Fibril cores and seeding interfaces are the same. (2) The overall timescale for de novo conversion is unperturbed. (3) The overall timescale of seeded IAPP_{WT} kinetics is rapid compared to

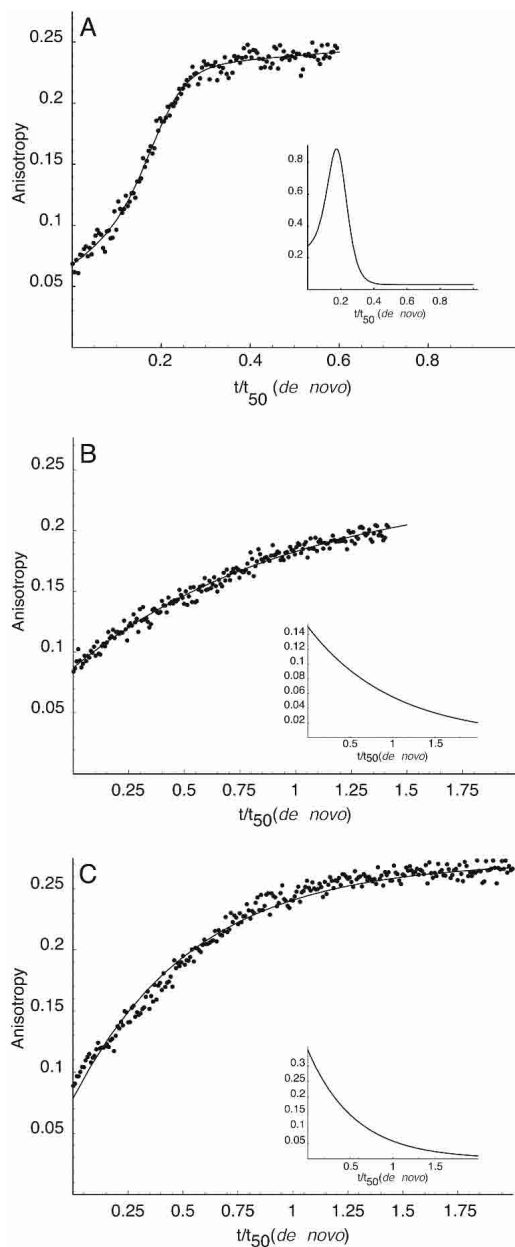


Figure 4. Self-seeded kinetics of fiber formation. In each sample, a 10 μM de novo reaction is seeded with 1 μM preformed fiber generated from the same variant. Each curve shown is a representative of a triplicate set of data. Shown are the raw data and corresponding fit for each reaction. (A–C) Seeded kinetics of fiber formation renormalized to the t_{50} s of the de novo counterparts by IAPP_{WT}, IAPP_{8–37}, and IAPP_{CAM}, respectively. The seeded kinetics of IAPP fiber formation and all de novo kinetics were fit to sigmoid transitions, and the seeded kinetics of IAPP_{8–37} and IAPP_{CAM} were fit to exponential models (see Materials and Methods). The *inset* to each figure shows the first derivative of the fits to each seeded kinetic plotted against a time axis renormalized to the t_{50} of the de novo counterpart. In such a plot, the sigmoidal kinetic profiles appear as a peak. The plots were generated by calculating the derivatives of the fits to the seeded and de novo kinetic data obtained for fiber formation reactions of each construct. The first derivative reflects the change in anisotropy per time step. The differences in initial anisotropies for the seeded reactions versus that of the de novo reactions can be accounted for as the contribution to anisotropy from having 10% (by mass) seed in solution.

de novo kinetics. By contrast, the seeded kinetic timescale of our constructs are comparable to their de novo kinetics. (4) The activation step evident in IAPP_{WT} is lost under our reaction conditions. (5) The sigmoidal transition in fibrillar conversion is significantly more abrupt in wild-type compared to modified constructs. (6) Deviations from IAPP_{WT} behavior are the same for both IAPP_{CAM} and IAPP_{8–37}.

The mechanism of assembly by IAPP_{CAM} and IAPP_{8–37} is the same as in IAPP_{WT}. This conclusion is derived from the observation that neither the core structure nor the de novo kinetics of assembly is greatly perturbed. Rather, our observables likely reflect simple alteration in the magnitude of constants associated with the wild-type assembly process. We therefore place our observations in the context of the phase-mediated fibrillogenesis (PMF) model previously described (Padrick and Miranker 2002). Briefly, upon initiation of fibrillogenesis by dissolution of IAPP into aqueous buffer, IAPP rapidly partitions into two phases. The first phase is soluble and actively participates in nucleation and elongation phenomena. The second phase is a dispersion with a characteristic size distribution and spread uniformly throughout the bulk solution. During the lag time of fibril assembly, this dispersion acts as a reservoir to maintain a fixed concentration of IAPP. As a result, the midpoints of fiber formation reactions, t_{50} , are insensitive to initial precursor concentration. Primary nucleation occurs by the association of soluble IAPP into oligomers that can convert to form fiber nuclei. These nuclei can be elongated by soluble IAPP to generate fibers. As the amount of fiber increases, secondary nucleation processes begin to dominate the reaction. Secondary nucleation is a process by which new fiber ends are formed in a manner dependent on the presence of pre-existing fibers. The result of secondary nucleation is rapid acceleration of fiber formation once a significant amount of fiber is present. The change from the lag period to the rapid transition period in IAPP fiber growth represents a shift in dominance from primary to secondary nucleation processes. The dispersed phase then takes a more active role in fibril conversion, since the maximum rate of conversion at t_{50} scales linearly with protein concentration. Several properties of dispersions vary linearly with protein concentration, enabling a rate-limiting step with linear concentration dependence. Our preferred description is that the release of soluble peptide from the dispersed phase becomes rate limiting during the elongation portion of fibrillogenesis. Such a release may or may not be coupled to the contact of dispersed phase elements with the ends of elongating fibers.

The removal of the disulfide bond eliminates the activation step in IAPP polymerization. Soluble IAPP assumes a random coil structure in aqueous solution as detected by far UV-CD (Kayed et al. 1999; Higham et al. 2000) and yet shows transient sampling of structure as detected by FRET (Padrick and Miranker 2001). The geometric constraints of

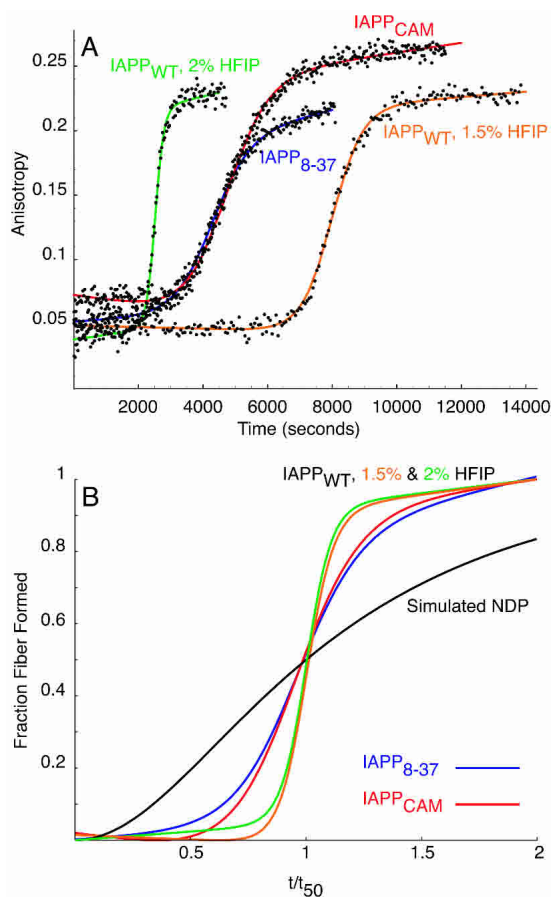


Figure 5. Raw and doubly renormalized profiles of de novo fiber formation. (A) Kinetic profiles of de novo fiber formation for IAPP_{WT}, IAPP₈₋₃₇, and IAPP_{CAM}. IAPP₈₋₃₇ and IAPP_{CAM} reactions were conducted at a concentration of 10 μ M soluble protein, 1.5% HFIP (v/v). Two separate wild-type IAPP de novo kinetics at two co-solvent percentages are shown (1.5% and 2% HFIP). (B) De novo fiber formation kinetic profiles for the three constructs are shown doubly renormalized and overlaid for comparison. Each curve was generated from a model with parameters obtained from a fit to a sigmoidal transition (see Materials and Methods). The time-axis was renormalized to the midpoint (t_{50}) of each curve, and the y-axis was renormalized to the ending anisotropy.

the intramolecular disulfide bridge could potentially influence the distribution of conformations sampled by IAPP within the dispersions. It is plausible that the establishment of an equilibrium between conformers takes place on the minute timescale. Within this context, the activation event evident in seeded kinetics (Fig. 1) may represent the establishment of this equilibrium. In the PMF model, the elongation of IAPP is impacted and moreover, eventually rate-limited by the release of IAPP from the dispersion. We suggest that both the conformations and rate of peptide release of IAPP from the dispersed phase are important to the rate of fiber elongation. In our two variants IAPP₈₋₃₇ and IAPP_{CAM}, we are no longer able to observe a biphasic kinetic. Elimination of the disulfide bond may simply corre-

spond to a simple reduction of the size of the distribution of states sampled by IAPP.

Loss of the disulfide bridge results in an apparent decrease in secondary nucleation processes. This is most readily observed as a change in the reaction profile (Fig. 5). A second consequence of secondary nucleation is marked acceleration by seeding. For IAPP_{WT}, seeded reactions complete before the t_{50} of the corresponding de novo reaction (Fig. 4A). In contrast, the seeded polymerization of IAPP₈₋₃₇ and IAPP_{CAM} follow an exponential fiber growth (Fig. 4B,C), which completes on a timescale comparable to the de novo reaction under our conditions. Within the PMF model and in the absence of secondary nucleation, the rate of fiber elongation is simply dependent on the rate-limiting release of monomeric IAPP from dispersions. Therefore, it is likely that this rate limit is accentuated in our seeded kinetics, resulting in elongation occurring on a timescale comparable to de novo conversion.

It is intriguing then that the N-terminal domain of IAPP affects two apparently distinct processes: the lag phase activation step and secondary nucleation. While these may be independent phenomena, it is possible to couple these observables if we assume (as above) a distribution of states accessible to IAPP within the dispersed phase. If two (or more) distinct conformers can be incorporated into a growing fiber, then the interface between conformers in the fiber could be regarded as a flaw in the fiber structure. Such a flaw could serve as a nucleus for lateral formation of new fibers, or may represent a weak position at which a fiber may break. In either case, this represents secondary nucleation as new fibers are formed in a manner dependent on preexisting fibers. Though the mechanism of secondary nucleation for IAPP polymerization is unclear, lateral association has been observed via AFM studies (Green et al. 2004). Regardless of the exact mechanism, the observation that IAPP₈₋₃₇ and IAPP_{CAM} de novo kinetics show a diminishment of secondary nucleation could reflect a perturbation in the distribution of such distinct states. Thus, it is plausible that activation and secondary nucleation phenomena are coupled in IAPP fibrillogenesis.

Here we report the first insights into the molecular nature of activation and secondary nucleation in IAPP fiber formation. Previous studies have implicated the role of distinct conformers in fiber formation of other amyloidogenic proteins. For instance, it has been suggested that favored and disfavored conformers exist for prion protein, and that such conformers have distinct rates of fiber elongation in vitro in fiber seeding experiments of heterogeneous mixtures of prion conformers (DePace and Weissman 2002). Additionally, it has been observed that conformational species barriers in prion proteins can be artificially generated or altered by point mutations (Chien et al. 2003) in the protein sequence. These findings as well as our studies support the idea that protein conformations can differentially affect the

mechanism of fiber assembly. Furthermore, our work demonstrates that peripheral domains of peptides that are not centrally involved in the fibril core can play a significant role in the mechanism of amyloid assembly. Finally, our work provides insight into the importance of secondary nucleation in fiber formation. Secondary nucleation is a readily evident and variable property of a number of amyloid systems. Since secondary nucleation affects the sharpness of amyloid transitions and seeding sensitivity, its presence is easily identified. For example, polymerization of Sup35-NM domain likely does not include secondary nucleation, as efficient seeding requires prior sonication of fiber seeds (Serio et al. 2000; Chien and Weissman 2001; DePace and Weissman 2002; Chien et al. 2003). Moreover, it has been suggested that the characteristic scission rates of prion polymers (intrinsic rate of polymer breakage) are essential to propagation and infectivity (Hall and Edskes 2004). The mechanism by which the presence of favorable and unfavorable conformers directs secondary nucleation is therefore of general importance to understanding the molecular basis of amyloid fibril assembly.

Materials and methods

Peptides and chemicals

1,1,1,3,3,3-hexafluoroisopropanol (HFIP) was obtained from Sigma-Aldrich and repurified by fractional distillation. Buffers and salts were obtained from J.T. Baker. All peptides used in this study were synthesized and purified in house via the W.M. Keck Foundation Biotechnology Resource Laboratory. IAPP_{CAM} was obtained by incubating purified wild-type IAPP in the presence of 13 mM DTT in 6 M GuHCl, 0.19M Tris HCl, 10% DMSO, pH 8.0 for 4 h at 4°C under nitrogen gas to facilitate the reduction of the intramolecular disulfide bond. The reduced peptide was then incubated with the 8 mM iodoacetamide at 4°C for 4 h under nitrogen gas in the dark. The labeling reaction was then quenched with 80 mM 2-mercaptoethanol. The subsequent purification of IAPP_{CAM} was performed by reverse-phase HPLC. Stock solutions of the three IAPP variants were made by solubilizing freeze-dried peptide in 7 M GuHCl, 10% DMSO, 0.1% TFA, filtered through 0.2-micron syringe filters (Pall Corp.), then loaded onto Vydac C-18 microspin columns (Amika/Harvard Bioscience). The peptide was bound to the column, washed with 10% acetonitrile, 0.1% TFA, and MilliQ water, and then eluted using HFIP. Concentrations of stock solutions in HFIP were determined by resuspending dried samples in 7 M GuHCl, pH 6.0 and measuring absorbance at 280 nm. Extinction coefficients of 1400 cm⁻¹M⁻¹, 1400 cm⁻¹M⁻¹, and 1280 cm⁻¹M⁻¹ were used for IAPP_{WT}, IAPP_{CAM}, and IAPP₈₋₃₇, respectively.

Fiber formation

Standard de novo reactions were prepared by diluting IAPP from a concentrated stock (stock concentrations ranged from 700 μM to 1.5 mM) in HFIP into an aqueous buffer solution resulting in final conditions of 25 μM IAPP in 50 mM potassium phosphate, 100 mM KCl, with 2.5% (v/v) co-solvent percentage at pH 7.4.

For seeded reactions, fiber seeds were generated by incubating 40 μM IAPP in 50 mM potassium phosphate, 100 mM KCl, pH 7.4 with 5% (v/v) HFIP for 30 min. These conditions led to reaction completion times of less than 15 min. After 30 min, the sample was diluted 1:1 with aqueous buffer containing 50 mM potassium phosphate and 100 mM KCl at pH 7.4 to generate 20 μM IAPP fibers in 2.5% HFIP. Seeds were aliquoted into a freshly prepared tube containing 10 μM IAPP, 1.5% HFIP at the beginning of the reaction. Final conditions were 10 μM IAPP monomer, 1 μM seed, 1.5% HFIP, 50 mM potassium phosphate, 100 mM KCl, pH 7.4.

Transmission electron microscopy

Micrographs of negatively stained IAPP fiber samples were imaged on a Phillips Tecnai 12 transmission electron microscopy at 120 kV accelerating voltages. Samples were prepared by aliquoting 5 μL of IAPP in aqueous buffer to a copper mesh grid freshly coated with carbon and glow discharged at 25 mA for 30 sec. Following incubation of sample on the carbon grid for 1 min, sample was wicked off and 5 μL of 1% (w/v) phosphotungstic acid (PTA) at pH 7.0 was applied onto the grid. Grids were incubated with PTA stain for 1 min and blot dried. Images were acquired using a 1000 × 1000 pixel Gatan 794 slow-scan CCD at a magnification of 15,000× and 5 μm underfocus. Image analysis was performed using Gatan DigitalMicrograph software.

Fluorescence spectroscopy

Fluorescence anisotropy measurements were performed using a two-channel fluorometer (Photon Technology International) with linear polarizers. Samples were excited at 278 nm wavelength with linearly polarized light, and fluorescence emission was detected at 303 nm at two polarized orientations, parallel and perpendicular to the polarization of the excitation channel. The cuvette temperature in the fluorometer was regulated to 25°C and maintained using a circulating water bath.

Data analysis

The kinetic anisotropy data, $r(t)$, were fit to either sigmoid or exponential models depending on the shape of the kinetic profile. Specifically, the de novo kinetics of fiber formation for all three IAPP variants (wild-type, IAPP₈₋₃₇, and IAPP_{CAM}) and the seeded kinetics of wild-type IAPP were fit to the following model:

$$r(t) = (m_1 \times t + r_1)A + (m_2 \times t + r_2)(1-A), \text{ where } A = (1 + e^{((50-t)/\tau)})^{-1},$$

r_1 and r_2 are lower and upper baselines, respectively, m_1 and m_2 are the slopes of the corresponding baselines.

The seeded kinetics of IAPP₈₋₃₇ and IAPP_{CAM} were fit to the following exponential model:

$$r(t) = e^{-kt} (r_1 - r_2) + r_2, \text{ where } r_1 \text{ is the initial anisotropy value at time, } t = 0 \text{ and } r_2 \text{ is the value of anisotropy at the upper baseline.}$$

The data fitting to the two models was performed using the NonlinearRegress function in Mathematica 4.2 (Wolfram Research). All reported data in this work are expressed as ± 1 SEM or ≥ 3 repeats.

Acknowledgments

We thank Dr. S. Jaswal and Dr. S.B. Padrick for helpful discussions and critical reading of the manuscript. We also thank Prof. V.

Unger for assistance with electron microscopy. This work was supported by a grant from the National Institutes of Health DK54899.

References

- Bucciantini, M., Giannoni, E., Chiti, F., Baroni, F., Formigli, L., Zurdo, J., Taddei, N., Ramponi, G., Dobson, C.M., and Stefani, M. 2002. Inherent toxicity of aggregates implies a common mechanism for protein misfolding diseases. *Nature* **416**: 507–511.
- Chien, P. and Weissman, J.S. 2001. Conformational diversity in a yeast prion dictates its seeding specificity. *Nature* **410**: 223–227.
- Chien, P., DePace, A.H., Collins, S.R., and Weissman, J.S. 2003. Generation of prion transmission barriers by mutational control of amyloid conformations. *Nature* **424**: 948–951.
- Come, J.H., Fraser, P.E., and Lansbury Jr., P.T. 1993. A kinetic model for amyloid formation in the prion diseases: Importance of seeding. *Proc. Natl. Acad. Sci.* **90**: 5959–5963.
- DePace, A.H. and Weissman, J.S. 2002. Origins and kinetic consequences of diversity in Sup35 yeast prion fibers. *Nat. Struct. Biol.* **9**: 389–396.
- Eanes, E.D. and Glenner, G.G. 1968. X-ray diffraction studies on amyloid filaments. *J. Histochem. Cytochem.* **16**: 673–677.
- Gazit, E. 2002. A possible role for pi-stacking in the self-assembly of amyloid fibrils. *FASEB J.* **16**: 77–83.
- Goldsbury, C., Goldie, K., Pellaud, J., Seelig, J., Frey, P., Muller, S.A., Kistler, J., Cooper, G.J., and Aebi, U. 2000. Amyloid fibril formation from full-length and fragments of amylin. *J. Struct. Biol.* **130**: 352–362.
- Green, J.D., Goldsberry, C., Kistler, J., Cooper, G.J., and Aebi, U. 2004. Human amylin oligomer growth and fibril elongation define two distinct phases in amyloid formation. *J. Biol. Chem.* **279**: 12206–12212.
- Hall, D. and Edskes, H. 2004. Silent prions lying in wait: A two-hit model of prion/amyloid formation and infection. *J. Mol. Biol.* **336**: 775–786.
- Harper, J.D. and Lansbury Jr., P.T. 1997. Models of amyloid seeding in Alzheimer's disease and scrapie: Mechanistic truths and physiological consequences of the time-dependent solubility of amyloid proteins. *Annu. Rev. Biochem.* **66**: 385–407.
- Higham, C.E., Jaikaran, E.T., Fraser, P.E., Gross, M., and Clark, A. 2000. Preparation of synthetic human islet amyloid polypeptide (IAPP) in a stable conformation to enable study of conversion to amyloid-like fibrils. *FEBS Lett.* **470**: 55–60.
- Kahn, S.E., Andrikopoulos, S., and Verchere, C.B. 1999. Islet amyloid: A long-recognized but underappreciated pathological feature of type 2 diabetes. *Diabetes* **48**: 241–253.
- Kayed, R., Bernhagen, J., Greenfield, N., Sweimeh, K., Brunner, H., Voelter, W., and Kapurniotu, A. 1999. Conformational transitions of islet amyloid polypeptide (IAPP) in amyloid formation in vitro. *J. Mol. Biol.* **287**: 781–796.
- Kubelka, J., Hofrichter, J., and Eaton, W.A. 2004. The protein folding “speed limit”. *Curr. Opin. Struct. Biol.* **14**: 76–88.
- Lakowicz, J.R. and Maliwal, B.P. 1983. Oxygen quenching and fluorescence depolarization of tyrosine residues in proteins. *J. Biol. Chem.* **258**: 4794–4801.
- O’Nuallain, B., Williams, A.D., Westermark, P., and Wetzel, R. 2004. Seeding specificity in amyloid growth induced by heterologous fibrils. *J. Biol. Chem.* **279**: 17490–17499.
- Oosawa, F. and Asakura, S. 1975. *Thermodynamics of the polymerization of protein*, p. 49. Academic Press, London, New York.
- Padrick, S.B. and Miranker, A.D. 2001. Islet amyloid polypeptide: Identification of long-range contacts and local order on the fibrillogenesis pathway. *J. Mol. Biol.* **308**: 783–794.
- . 2002. Islet amyloid: Phase partitioning and secondary nucleation are central to the mechanism of fibrillogenesis. *Biochemistry* **41**: 4694–4703.
- Plaxco, K.W. and Dobson, C.M. 1996. Time-resolved biophysical methods in the study of protein folding. *Curr. Opin. Struct. Biol.* **6**: 630–636.
- Rochet, J.C. and Lansbury Jr., P.T. 2000. Amyloid fibrillogenesis: Themes and variations. *Curr. Opin. Struct. Biol.* **10**: 60–68.
- Santoso, A., Chien, P., Osherovich, L.Z., and Weissman, J.S. 2000. Molecular basis of a yeast prion species barrier. *Cell* **100**: 277–288.
- Serio, T.R., Cashikar, A.G., Kowal, A.S., Sawicki, G.J., Moslehi, J.J., Serpell, L., Arnsdorf, M.F., and Lindquist, S.L. 2000. Nucleated conformational conversion and the replication of conformational information by a prion determinant. *Science* **289**: 1317–1321.
- Sunde, M. and Blake, C. 1997. The structure of amyloid fibrils by electron microscopy and X-ray diffraction. *Adv. Protein Chem.* **50**: 123–159.